Plasmon-induced hot carrier transfer to the surface of three-dimensional topological insulators

Hari P. Paudel,[1,*] Vadym Apalkov,[1] Xiaojuan Sun,[2] and Mark I. Stockman[1,†]
[1]*Department of Physics and Astronomy, Center for Nano-Optics, Georgia State University, Atlanta, Georgia 30303, USA*
[2]*State Key Laboratory of Luminescence and Applications, Changchun Institute of Optics, Fine Mechanics and Physics, Changchun 130033, China*

(Received 5 September 2017; revised manuscript received 12 April 2018; published 27 August 2018)

We consider theoretically a conical Ag tip coupled to surface states of a three-dimensional topological insulator (3D TI) such as Bi_2Se_3. Generation of propagating surface plasmon polaritons (SPPs) in a metal cone by a laser field produces an intense optical field near the tip of the cone and high concentration of hot carriers in the metal near the surface of the topological insulator. Such hot carriers are transferred through a Schottky contact between tip and TI to the chiral spin surface states of TI, resulting in finite spin polarization and spin current at the surface of TI. SPPs in the metal cone are excited with a THz laser with energy in the optical band gap of 3D TI to avoid photoexcitations in the bulk of Bi_2Se_3. We also propose a detail scheme for experimental measurements of such currents. Our results can find applications in spintronics.

DOI: 10.1103/PhysRevB.98.075428

I. INTRODUCTION

In a nanosystem of a size larger than the nonlocality radius, $l_n \sim \upsilon_F/\omega$, the radiative decay of SPPs is highly suppressed, and SPPs transfer most of their energy to valence band electrons creating "hot" carriers. It has been shown that decay of SPPs can generate strong photocurrent in plasmonic nanoantennas/semiconductor interface [1,2]. An unprecedented level of optical energy accumulation can be achieved at the tip, and generated hot carriers after decay of SPPs can be used for the purpose of nanoscopy based on atomic force microscopy in scanning the surface of a material below spatial resolution of 50 nm [3]. Significant energy transfer from SPPs to single electron excitations occurs for nanosystems (nanocrystals) with a size around 10 nm [4,5].

The decay rate of SPPs is inversely proportional to radius R of a plasmonic nanocone if R is less than the skin depth of metals, $l_s = \frac{\omega}{c}[Re(\frac{-\varepsilon_m^2}{\varepsilon_m+\varepsilon_d})]$, where ε_m and ε_d are the metal and medium dielectric parameters, respectively (for Ag and Au, $l_s \sim 25$ nm) [6–9]. Due to a strong filed enhancement, accumulation of energy can be obtained to a scale of size of the nonlocality radius, which is around a nanometer. The SPPs propagating towards the tip are adiabatically concentrated, and the optical energy is focused along tapered waveguides at the dimension of nonlocality radius. The group velocity of SPPs, $\upsilon_g = \frac{1}{\hbar}\frac{dE_q}{dq}$, asymptotically decreases along waveguides, which leads to a highly localized field at the conical tip [7,8]. SPPs in nanocylinders or nanorods of noble metals at terahertz frequency (THz) are shown to have propagation length in millimeter range [10,11].

If wave vector $\mathbf{q}$ ($\mathbf{q} \leqslant \mathbf{0.3}$ L, where L is a high symmetry point of the first Brillouin zone of Ag) of SPP is small compared to electron's momentum, then SPP's energy, that is transferred to s electrons, is an energy difference between the states $\mathbf{k}$ and $\mathbf{k}+\mathbf{q}$, $E_{\mathbf{k}+\mathbf{q}} - E_{\mathbf{k}} \approx \frac{\hbar^2}{m}\mathbf{q}\cdot\mathbf{k}$. This energy difference is below the interband threshold E_{th} (in Ag, $E_{\text{th}} = 3.7$ eV). Hot carriers with longer lifetime (and mean free path of up to 40 nm) are generated after decay of SPPs with energy lower than the interband threshold. Above E_{th}, generated hot carriers are short lived and are excited mostly from d bands with the mean free path of 5 nm or smaller [12]. Therefore, in noble metals the interband threshold separates two regimes of hot carrier excitations. In a conical waveguide with tip size a, SPPs characteristic wavelength is equal to the size of the tip's circumference and maximum energy transferred to hot carriers is about $\frac{\hbar^2}{m}qk$. If we assume that the plasmonic fields result in the transitions around the Fermi level in metal, then the energy transferred to hot carriers is $\hbar\upsilon_F q \approx 0.3$ eV for a tip of size $a = 4$ nm.

The spins of SPPs induced carriers in a metal tip are randomly oriented. Such carriers are injected on a surface of 3D TI with spin chiral states, which results in a spin polarized surface current due to nonequilibrium carrier distribution and spin-momentum locking property of TI surface states. In Ref. [13], authors propose a model for a topological plasmon spin filter that utilizes THz spin plasmons on the surface of 3D TI to generate a static spin accumulation in resonant Ag metallic nanostructures coupled to the 3D TI. In one half cycle of plasmonic field, a spin-up is induced while in the other half cycle a spin-down is induced in the Ag metal. Spins are then driven away in opposite directions by a drift. This possibility shows that 3D TI can be a source of polarized spin current without a need of external drift. In this paper, we propose another approach to generation of spin polarization at the surface of 3D TI coupled to the metal conical tip. The idea is based on adiabatic concentration of SPPs at the end of the tip. We consider hot carriers are generated after the decay of SPPs in a conical Ag waveguide of base radius R and length L. The induced hot carriers are transferred to a surface of 3D TI material such as Bi_2Se_3, generating a spin

*Hari.paudel@netl.doe.gov
†mstockman@gsu.edu

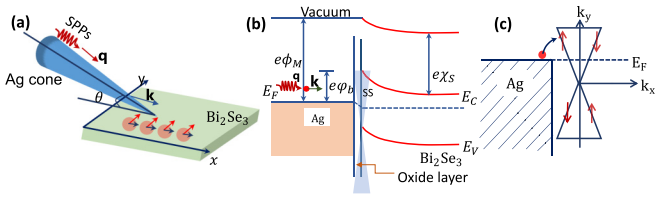

FIG. 1. Schematic of (a) an Ag cone placed over a Bi_2Se_3 surface with an orientation angle of θ. SPs are excited and decay inducing hot carriers, which are injected to the surface of Bi_2Se_3, and (b) the band alignments at the Ag/Bi_2Se_3 interface. The side view of the Dirac cones are also depicted to show surface states (SSs), and (c) SPP decay induced carriers with energy $E_F \leqslant E \leqslant E_F + e\varphi_b$ and spin component S_y are filling single particle Dirac states.

polarized current with density of up to 10^4 A/cm^2. Our result for the spin polarized current for a finite sheet of 3D TI with the given surface area is in the same order of magnitude (few micro amperes) as of the current obtained in the experiments [14]. We assume that the system is irradiated with a laser of wavelength 6 μm (≈0.2 eV) that selectively excites SPPs and does not photoexcite 3D TIs as the laser energy is within the optical band gap of Bi_2Se_3 [15]. Below the optical band gap of Dirac system, direct transitions are prohibited as the bands are filled up to the Fermi level. For the energy of photon $\hbar\omega \leqslant 2E_F$, photoexcitation does not occur in the 3D TI [16,17]. The 3D TIs are small band-gap semiconductors with metallic surface states. The energy dispersion of such surface states is the same as the energy dispersion of relativistic Dirac fermion, and the spin is locked in the direction perpendicular to the momentum [15,18,19]. Coupling between optical field and electrons in the metal tip induces long lived carriers through intraband transitions in Ag [12,20]. When the tip is placed near the surface of Bi_2Se_3, a nanoschottky diode is formed at the interface with a potential height of $e\varphi(\mathbf{r})|_{r=0} = e\varphi_b$ [21]. This potential difference is asymptotically equal to a difference of the work functions, $e\phi_{\rm Ag} - e\chi_{\rm Bi_2Se_3} = 0.2$ eV, between the two materials [Fig. 1(b)] (work function of a clean sample of Bi_2Se_3 is ≈4.23 eV [22]). The SPPs decay generates a nonequilibrium distribution of the carriers in the metal around the Fermi level. Such carriers are transferred into the surface of TI, which is characterized by single particle relativistic dispersion relation, see Fig. 1(c). Our system consists of an Ag conical tip of dimension $a \ll \sqrt{A}$, where A is the area of the surface of Bi_2Se_3. The tip angle is 0.08 rad. The waveguide is placed with a small angle orientation as shown in Fig. 1(a) that allows a maximum momentum transfer from metal to the surface of 3D TI. Due to a nanosize of the tip, we assume that single particle electron states at the surface of TI are unperturbed. In addition to that, the metal tip is not in complete contact with the surface of TI and therefore, it is sufficient to treat the situation under a regime of weak coupling of metal and Dirac states of Bi_2Se_3 [21,23,24]. This approximation is also valid in optical experiments, where the surface states are weakly coupled to the photoexcited bulk carriers [25–27].

The paper is organized as follows: We present our model based on the density matrix formalism in Sec. II. In Sec. III, we calculate the SPP fields propagating in a conical waveguide and show explicitly the field intensity developed at the tip. Section IV is devoted to the interaction of the SPP field with the metal electrons around the tip. We calculate the density of electrons that can be excited as a result of SPP decay. In Sec. V, descriptions of the SPP induced excited electrons that are moved to the interface and are transferred to the surface are presented. Finally, we summarize our paper with conclusions in Sec. VI.

II. MODEL BASED ON DENSITY MATRIX FORMALISM

Consider a Hamiltonian for our system as

$$H(t) = H_o + V(t), \tag{1}$$

where H_o is a time independent state Hamiltonian with eigenvalue E^o and $V(t)$ is a time varying potential which induces transitions between the eigenstates of H_o. The light matter interaction on the metal surface can be described by the term $V(t)$.

The Liouville equation to be solved is [28]

$$\hbar\frac{\partial\rho(t)_{mn}}{\partial t} = i[\rho(t)_{mn},\ H] + \left.\frac{\partial\rho(t)_{mn}}{\partial t}\right|_{\rm decay}, \tag{2}$$

where $\Gamma_{mn} = \frac{\hbar}{\tau_{mn}}$ is a relaxation rate between m^{th} and n^{th} states, and the decay term $\frac{\partial\rho(t)_{mn}}{\partial t}|_{\rm decay} = -\Gamma_{mn}(\rho(t)_{mn} - \rho(0)_{mn})$ describes the vacuum fluctuations or spontaneous emission. Diagonal terms of the Liouville equation are given by

$$\dot\rho_{mm}\ (t) = \Gamma_{mm}\delta\rho_{mm}(t) + \frac{i}{\hbar}\sum_{m\neq n}(\rho_{nm}(t)V_{mn}(t) - V_{nm}(t)\rho_{mn}(t)), \tag{3}$$

where $\delta\rho_{mn}(t) = \rho_{mn}(t) - \rho_{mn}(0)$. Any diagonal term of $V(t)$ just renormalizes E^o. The off diagonal term of the density matrix is given by

$$\dot\rho_{mn}\ (t) = \frac{i}{\hbar}\rho_{mn}(t)\left(E^o_n - E^o_m\right) + \frac{i}{\hbar}V_{mn}(t)(\rho_{mm}(t) - \rho_{nn}(t)) - \Gamma_{mm}(\rho(t)_{mm} - \rho_{nn}(0)). \tag{4}$$

To find the population density, $\delta\rho_{mm}$, on the surface of metal, the solution of interest is the diagonal element of density matrix, which can be solved under rotating wave approximation.

In the interaction picture, the off diagonal term is

$$\rho_{mn}(t) = \rho^I_{mn}(t)e^{-\frac{i}{\hbar}(E^o_n - E^o_m)t}. \tag{5}$$

This implies

$$\hbar\dot\rho^I_{mn}(t) = -\hbar\Gamma_{mm}\rho^I(t) - iV_{mn}(t)(e^{i(\omega t+\omega_{mn}t)} + e^{i(\omega t-\omega_{mn}t)})(\rho_{nn}(t) - \rho_{mm}(t)), \tag{6}$$

where $V_{mn}(t) = V_{mn}(e^{-i\omega t} + e^{i\omega t})$. The density matrix can be written in two components form as $\rho^I_{mn}(t) = (\rho^{I,a}_{mn}(\omega)e^{-i\omega t} + \rho^{I,b}_{mn}(\omega)e^{i\omega t})e^{i\omega_{mn}t}$. Under adiabatic pumping $\rho(t) \to \rho(\omega)$, and rotating wave approximation, the term with $e^{i(\omega t+\omega_{mn}t)}$ can be discarded. This implies that the components

of the density matrix can be written as [28]

$$\rho^{I,a}_{mn}(\omega) = \frac{|V_{mn}|\left(\rho^{I}_{nn} - \rho^{I}_{mm}\right)}{\hbar\omega - \hbar\omega_{mn} + i\,\Gamma_{mn}\hbar} \tag{7}$$

$$\rho^{I,b}_{mn}(\omega) = \frac{|V_{mn}|\left(\rho^{I}_{nn} - \rho^{I}_{mm}\right)}{-\hbar\omega - \hbar\omega_{mn} + i\,\Gamma_{mn}\hbar}. \tag{8}$$

When a dynamic equilibrium is established, the rate of change of the density matrix with respect to time approaches to zero, $\dot{\rho}_{mm}(t), \dot{\rho}_{nn}(t), \to 0$. Under this situation the stimulated emission and absorption are balanced by the relaxation process [28]. With the help of equations (7) and (8), we can write the off diagonal density matrix elements in frequency space. Then using equations (3) and (4), the nonequilibrium population density can be obtained as

$$\delta\rho_{mm}(t) = -\frac{2}{\Gamma_{mm}}\sum_{m\neq n}(\rho_{nn} - \rho_{mm})|V_{mn}|^2 \times\left[\frac{\Gamma_{mn}}{(\hbar\omega - \hbar\omega_{mn})^2 + (\Gamma_{mn}\hbar)^2} + \frac{\Gamma_{nm}}{(\hbar\omega + \hbar\omega_{mn})^2 + (\Gamma_{nm}\hbar)^2}\right], \tag{9}$$

where we drop the index I. Note that $\delta\rho_{mm}(t) = -\delta\rho_{nn}(t)$. Two terms on the right hand side of equation (9) describe the emission and absorption process between the states n^{th} and m^{th}.

III. SPP FIELD IN CONICAL WAVEGUIDE

The matrix elements V_{mn} are determined by interaction between the plasmonic field and the single electron system in the metal. We solve for radial and longitudinal components of the plasmonic field in metal under the condition of adiabatic focusing of the field in the tip. Following Ref. [7], Maxwell's equation required to solve in the cylindrical coordinates for TM modes $H_\theta = \phi(\xi)\psi(z)$ are

$$\xi^2\frac{\partial^2\phi}{\partial\xi^2} + \frac{1}{\xi}\frac{\partial\phi}{\partial\xi} - \left(1 + \beta^2\xi^2k_o^2\right)\phi = 0 \tag{10}$$

$$\frac{\partial^2\psi}{\partial z^2} + n^2 = 0, \tag{11}$$

where $\beta = \sqrt{n^2 - \epsilon}$, and n is the index of refraction that is a function of z. With $r = \beta\xi k_o$, solutions

$$\phi_< = A\ I_1(r_<) \tag{12}$$

$$\phi_> = B\ K_1(r_>), \tag{13}$$

where A and B are the field amplitudes, respectively, inside and outside the metal surface. $K_n(I_n)$ are the n^{th} modified Bessel function of the second (first) kind. The solutions for magnetic field can be written as $H_\theta(r_<) = \phi(r_<)\psi(z)$ and $H_\phi(r_>) = \phi(r_>)\psi(z)$, where $r_>(r_<)$ is greater (smaller) than R. Electric field can be calculated using $\frac{\partial E_r}{\partial t} = -\frac{c}{\epsilon_i}\frac{\partial H_\theta}{\partial t}$ and $\frac{\partial E_z}{\partial t} = \frac{c}{r}\frac{\partial r H_\theta}{\partial t}$ with the time varying components. Using boundary condition $E_{z1} = E_{z2}$ and $\epsilon_1 E_{z1} = \epsilon_2 E_{z2}$, we obtain the condition

$$\frac{\epsilon_2}{\beta_2}\frac{K_1}{K_o} + \frac{\epsilon_1}{\beta_1}\frac{I_1}{I_o} = 0, \tag{14}$$

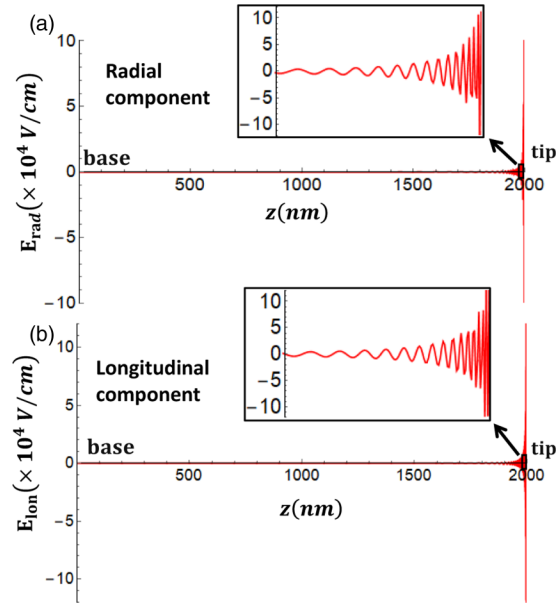

FIG. 2. The total electric field distribution of (a) radial component and (b) longitudinal component in a Ag conical waveguide. The length of the cone is 2000 nm, and SPPs are propagating from base to tip in vacuum. The insets show the fields near the tip in enlarged scale. The simulation stops at 2 nm away from the tip.

where ϵ_1 and ϵ_2 is the dielectric function of environment and that of metal. The R dependence of the index of refraction n is obtained by solving the equation (14). Under the asymptotic limit of the modified Bessel function we obtain

$$n = \sqrt{\frac{4}{k_o^2R^2}\left(\frac{\epsilon_1/\epsilon_2}{W[e^{2\gamma}\epsilon_1/\epsilon_2]}\right) + \epsilon_1}, \tag{15}$$

where $\gamma \approx 0.577$ is a Euler constant and W is Lambert's function. The R dependence of n increases rapidly as we approach to the tip. In Fig. 2 we show the electric field amplitude of SPPs propagating along the conical waveguide. Near the tip accumulation of energy is obtained at the unprecedented level.

IV. INTERACTION OF SPP WITH ELECTRONS IN METAL TIP

The second quantization expression for the electric field of SPP has the following form

$$\mathbf{E} = \sum_{\mathbf{q}}\mathbf{E}_{\mathbf{q}}(r)(a^+_{\mathbf{q}} + a_{\mathbf{q}}). \tag{16}$$

The interaction potential is given by

$$V_I = \sum_{\mathbf{q},\mathbf{k}}\Omega_{\mathbf{k},\mathbf{q}}(b^+_{c,\mathbf{k}-\mathbf{q}}b_{v,\mathbf{k}}c^+_{\mathbf{q}} + b^+_{v,\mathbf{k}+\mathbf{q}}b_{c,\mathbf{k}}c_{\mathbf{q}}), \tag{17}$$

where

$$\Omega_{\mathbf{k},\mathbf{q}} = \frac{ie}{m\omega_{k,k'}}\int\Psi^*_{c,\mathbf{k}'}\mathbf{E}_{\mathbf{q}}\cdot\mathbf{P}\Psi_{v,\mathbf{k}}d^3\mathbf{r}. \tag{18}$$

Consider a simple model where electrons are trapped in a box with infinitely high potential wall, $V(r) = \infty$. Then the solutions of the Schrodinger equation in cylindrical coordi-

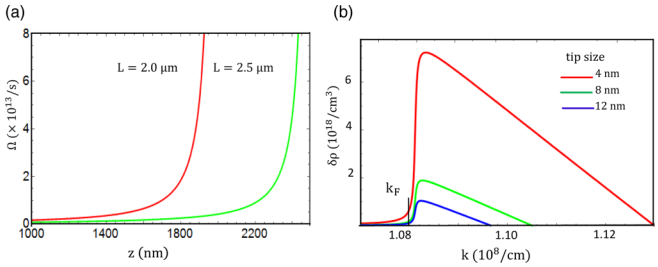

FIG. 3. (a) Carrier generation rates after SPPs decay. As an example, for length $L = 2000$ nm (red) and 2500 nm (green) are shown. As SPPs reach towards the tip, generation rate per unit length is higher. (b) The population density around the tip for $L = 2000$ nm conical waveguide at different sizes of the tip.

nates can be written as

$$\Psi_{n,l} = C_{n,l} e^{i\theta} \sin\left(\frac{n\pi}{L} z\right) J_l(\mu\xi), \tag{19}$$

where m^{th} zero of the Bessel function J_l is $\mu_{l,m} = \frac{z_{l,m}}{R(z)} l = 0,\ 1\ ,\ 2,\ 3....$, and $C_{n,l}$ are the amplitudes of the wave function. The corresponding energy eigenvalues are

$$E_{l,m} = (\hbar^2/2m)\left(z_{l,m}^2/R^2 + n^2\pi^2/L^2\right). \tag{20}$$

Consider, as an example, $z_{l,m} = 30$, $n = 5$, and a short waveguide with $L = 10$ nm. We obtain energy $E_{l,m} \approx 40$ meV at $R = 40$ nm. For a larger value of L, the wave vector k_z can be considered as a continuous variable. Therefore, only a sufficiently high value of quantum numbers contribute, which means the excitations happen close to the Fermi level. For a given state with quantized wave vector $k_z = \frac{n\pi}{L}$, the contribution to $\Omega_{\mathbf{k},\mathbf{q}}$ comes from the longitudinal field component, and it is nonzero only when the initial quantum number m_i and the final quantum number m_f are even and odd, and vice versa. On implementing a propagating solution for a long waveguide, we obtain a nonzero contribution from the radial component in addition to the longitudinal component of the field. Figure 3(a) shows the effect of decreasing of $R(z)$ on the excitation rate $\Omega_{\mathbf{k},\mathbf{q}}$ that describes the number of carriers generated per second. The results are shown for two different lengths of waveguide. It is to be noted that if the radius of the waveguide is less than the electron's mean free path, then SPPs lifetime is suppressed due to surface scattering and related size effects that can reduce τ_p by up to a factor of 5 [29].

Taking into account the symmetry of the problem, we adopt a cylindrical coordinates system to solve for the net excitation density of metal electron at the interface. The angle ϕ at which a plasmon's wave vector is scattered by an electron is in the range $\frac{k^2-k_F^2+q^2}{2kq} \leqslant \cos\phi \leqslant 1$. The energy difference $\hbar\omega_{\mathbf{k}+\mathbf{q},\mathbf{k}} = E_{\mathbf{k}+\mathbf{q}} - E_{\mathbf{k}}$ determines the group velocity of the SPPs. SPPs with the momentum satisfying the above conditions can produce a plasmon drag effect on the surface of 3D TI [30]. The SPP momentum in the radial direction is highly confined near the tip due to its one-dimensional nature of propagation along the cone axis. For states defined by the indices m and n in equation (9), the population density can be equivalently written in k space. A plasmon with momentum $\mathbf{q}$ can scatter an electron with initial momentum $\mathbf{k}$ to final momentum $\mathbf{k} + \mathbf{q}$. Hereafter we use k space indexing rather than indexing the state by m and n as these are two equivalent pictures. To simplify equation 9, we assume $\Gamma_{mn} \approx \Gamma_{mm} = \Gamma_{nn}$. The denominator of the density matrix becomes a real quantity defining the detuning from the resonance and depends not only on the scattering wave vector but also on the scattering angle. With the help of equations (17) and (18), equation (9) for the hot carriers density can be recast in terms of Rabi frequency. Here we calculate the hot carriers density around the tip and write the diagonal element of density matrix given by equation (9) as

$$\delta\rho_k = = \frac{2}{(2\pi)^3}\frac{1}{\hbar\omega} k_r^2 |\Omega_{\mathbf{k},q}|^2 \int_\theta \cos\theta d\theta \int_k dk \int_\phi \times \frac{d(\cos\phi)}{\left(\hbar\omega - \frac{\hbar^2 kq\cos\phi}{m} - \frac{\hbar^2 q^2}{2m}\right)^2 + \Gamma^2\hbar^2}, \tag{21}$$

where ϕ has limits of $\phi_{\min} = \frac{k^2-k_F^2+q^2}{2kq}$ and $\phi_{\max} = 1$. The limit over k is determined by the momentum conservation restricted by the value of $\cos\phi$. k_r is the wave vector in the radial direction. θ is the orientation of the cone with respect to the surface, and it is integrated to be unity. Integrations in equation (21) are readily performed to obtain

$$\delta\rho_k = \frac{2}{(2\pi)^3}\frac{1}{\hbar\omega} k_r^2 |\Omega_{\mathbf{k},q}|^2 \frac{m}{\hbar^2 q} \log\left(\frac{k_f}{k-q}\right)\Theta(k - k_F), \tag{22}$$

where $\Theta(...)$ is the Heavyside step function that determines the lower cutoff limit for the wave vector of the carrier. The momentum conservation is explicitly satisfied by taking into account the plasmon-electron scattering angle ϕ. Equation (22) shows that excitation density has logarithmic dependence on $(k_f/k - q)$. For $k \to k_f$ and $q \ll k$, we obtain $\delta\rho_k \to 0$. The excited carriers are distributed within a narrow region of k space above the Fermi wave vector ($k_F = 1.08 \times 10^8$/cm) as shown in Fig. 3(b). This region corresponds to the energy range of $E_F \leqslant E \leqslant e\varphi_b$. Figure 3(b) also shows the excited carrier density for different tip sizes.

V. INJECTION INTO TOPOLOGICAL SURFACE STATES

In Sec. IV, we calculated the density of excited hot carriers in metal after the decay of SPPs. The excitation density of hot carriers given by equation (22) can be injected into the topological surface states if the surface density of state is known. Only those carriers that are injected below the gap of 3D TI have a possibility of retaining the Dirac particlelike features. The number of carriers injected into the topological surface states with the wave vector $\mathbf{k}$ along the x direction can be written as $\delta\eta = g(E)\mathcal{D}_{\text{Dirac}}\Delta E$, where $\mathcal{D}_{\text{Dirac}}$ is the 2D density of states for Dirac fermions, ΔE is the energy interval of Dirac single particle states in the range of Δk, and $g(E)$ is the carrier distribution. The carrier distribution $g(E)$ is obtained by normalizing $\delta\rho_k$ from equation (22) with the total number of possible excitations within the range of E_F and $E_F + e\varphi_b$, and it can be written as $g(E) = \delta\rho_k / \frac{3}{2}\left(\frac{N}{V}\right)\int_E \frac{1}{E_F}\left(\frac{E}{E_F}\right)^{1/2} dE$ [31], where $N/V \approx 10^{22}/\text{cm}^3$. In 2D, $\mathcal{D}_{\text{Dirac}} = \frac{|E|}{2\pi(\hbar v_f)^2}$, where $v_F \approx 6 \times 10^5$ m/s is the Fermi velocity for Bi_2Se_3. The carrier

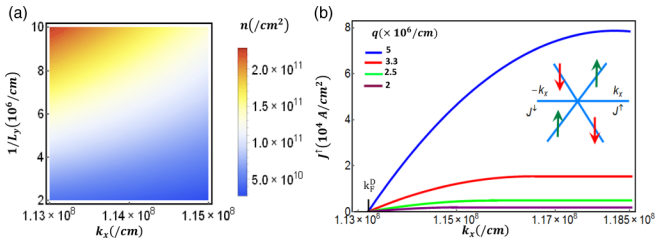

FIG. 4. (a) Carrier distribution on the surface of Bi_2Se_3 after the injection and is plotted as a function of k_x and inverse of the sample's length along the y axis. (b) Current density due to spin polarized carriers on the Dirac bands of the surface of Bi_2Se_3 as a function of the Dirac fermion wave vector at different SPPs wave vectors at the tip. The current density is obtained above the Fermi wave vector $k_F^D = E_{\mathbf{k}}/\hbar\upsilon_F$. Note that energy is measured from the vacuum level. The inset shows the scheme of spin polarization on the Dirac bands.

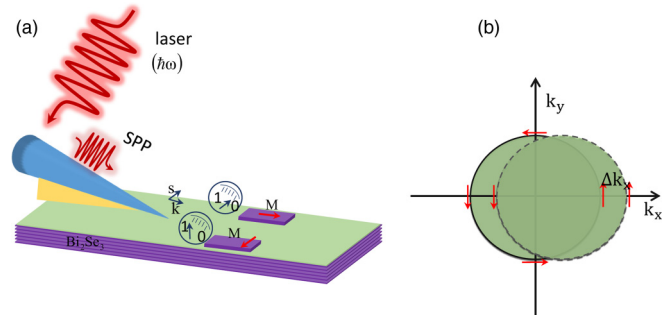

FIG. 5. Experimental setup to measure the enhanced spin polarized current on the surface of Bi_2Se_3 due to SPPs decay induced hot carriers. (a) Two ferromagnetic detectors on the surface measure the voltage proportional to projection of the 3D TI spin polarization onto the magnetization axis. (b) A small shift of Δk of the circular Fermi surface along $+\mathbf{k}_x$ generates current with spin along $+\mathbf{k}_y$.

distribution is limited in the y direction for fix k_y. The 2D density of state is inverse L_y dependent, $\mathcal{D}_{\text{Dirac}} = 1/L_y\hbar\upsilon_F$. We need particle flux traveling with momentum k_x whose spin is locked along k_y and passing through a strip of length k_y in the reciprocal space. Using the energy $E \approx \hbar\upsilon_f k$ of an electron around the Dirac point on the Fermi surface, we write the density of carriers injected into the surface of 3D TI in the longitudinal direction (x axis) as

$$\delta\eta = \frac{\delta\rho_k}{2}\frac{V}{N}\frac{E_F^{3/2}}{\left\{(E_F+e\phi)^{3/2}-E_F^{3/2}\right\}}\frac{1}{L_y\hbar\upsilon_F}e\varphi_b, \qquad (23)$$

where the factor $1/2$ is due to two states of spin, and only half the number of electrons are traveling to the $+x$ axis. Note that L_y is the length of the Bi_2Se_3 sample along the y direction, and $\delta\rho_k$ is given by equation (22). Due to the well defined momentum direction of a single particle Dirac state in a reciprocal space, only those hot electrons having a tangential momentum direction with nearly overlapping spin components to the Dirac states are injected. The electrons with spin-up (spin-down) polarization contribute to the electron current along $+\mathbf{k}_x$ ($-\mathbf{k}_x$). The polarized current density, $J_x^{\uparrow}$, for spin up states can be written as $J_x^{\uparrow} = e\upsilon_F\int\delta\eta^{\uparrow}$, where $\delta\eta^{\uparrow}$ is the density of spin up carriers. $J_x^{\uparrow}$ can be explicitly written as

$$J_x = \frac{1}{2}e\upsilon_F\frac{2}{(2\pi)^3}\frac{1}{\hbar\omega}k_r^2|\Omega_{\mathbf{k},q}|^2\frac{m}{\hbar^2 q}C\frac{1}{L_y\hbar\upsilon_f}\varepsilon_F\left(\frac{k'}{k_f}-\frac{k_f'}{k_f}\right), \qquad (24)$$

where $k' = k + (k-q)\log[k_f/(k-q)]$ and $k_f' = k_f + (k_f-q)\log[k_f/(k_f-q)]$, and $C = V/N(\frac{\varepsilon_F^{3/2}}{(\varepsilon_F+e\varphi_b)^{3/2}-\varepsilon_F^{3/2}})$ is a normalization factor.

Similarly, the expression for the spin down component contributing to the electron current along $-\mathbf{k}_x$ has the form $J_x^{\downarrow} = -e\upsilon_F\int\delta\eta^{\downarrow}$, where the negative sign is due to the opposite direction of Fermi velocity. In Fig. 4(a), we show carrier distribution on the surface of Bi_2Se_3 at different inverse length scales along the y axis after the injection, and in Fig. 4(b), we show $J_x^{\uparrow}$ on the surface of Bi_2Se_3 as a function of electron wave vector for $|\mathbf{k}_y| \approx 1/L_y = 0.017/\text{nm}$ and at different values of SPP momentum. The group velocity of SPP approaches zero and the wavelength is equal to the tip's circumference. Excited carriers above the metal Fermi surface with energy $E_F \leqslant E_k \leqslant E_F + e\varphi_b$ are passed to the semiconducting surface through the oxide layer with thickness of around one nanometer and energy barrier height of nearly 3 eV [3], see Fig. 1(b). The magnitude of Dirac fermion's wave vector is determined as $|\mathbf{k}^D| = E_{\mathbf{k}}/\hbar\upsilon_F$. Note that $k_D \geqslant k_F$, and k_D is calculated so as to satisfy the energy conservation across the interface. The spin polarized current is generated due to a shift of the center of the circular Fermi surface by Δk_F along $+\mathbf{k}_x$.

The in-plane group velocity υ_g of the Dirac fermions is a spin dependent quantity. From the low energy Dirac Hamiltonian, $H_k = \hbar\upsilon_f(\mathbf{z}\times\sigma)\cdot\mathbf{k}-\mu$, it can be obtained that $\upsilon_g = \frac{1}{\hbar}\frac{\partial H_k}{\partial k} = \frac{2}{\hbar}\upsilon_f(\mathbf{z}\times\mathbf{S})$, where $\mathbf{S} = \frac{\hbar}{2}\sigma$. If $\mathbf{S}$ is along $+\hat{\mathbf{y}}$, it is apparent that υ_g points along $+\hat{\mathbf{x}}$, a direction of the charge flow. The average spin polarizations along $+\hat{\mathbf{y}}$ is given by $\langle\mathbf{S}_y\rangle = \frac{\hbar}{2e\upsilon_f\eta}J_x$. Thus, a flow of spin polarized charges creates a net average spin accumulation in the direction perpendicular to the flow. Even a low carrier transfer efficiency can create a significant charge current across the interface [3], which in turn is proportional to the spin accumulation.

To measure $J^{\uparrow}(J^{\downarrow})$ experimentally, we propose a simple scheme as shown in Fig. 5. The photon energy of the laser that lunches SPPs in the Ag conical waveguide is chosen to be $\hbar\omega < 2\hbar\omega_{\text{opt}}$, where ω_{opt} is the optical band-gap frequency of 3D TI ($\hbar\omega \leqslant 0.2$ eV), to avoid photoexcitations on the surface and in the bulk of 3D TI. A thin film of Al_2O_3 is grown on a sample of Bi_2Se_3 film. Two spin sensitive ferromagnetic probes (such as Fe/Al_2O_3) are placed on the surface that detects spin polarized electrical current. This technique successfully enables electrical detection of the spin polarization in semiconductors and metals [14,32–34]. The ferromagnetic detector records the full spin signal proportional to the unpolarized charge current for electrons when the spins on the surface are polarized in an opposite direction to the contact magnetization direction (note magnetic moment $\mathbf{m}_s$ is in the direction of magnetization $\mathbf{M}$). As we rotate the direction of $\mathbf{M}$ in the x-y plane at the ferromagnetic contact, the spin signal decreases and becomes zero when $\mathbf{M}$ perfectly aligns

with the direction of momentum (orthogonal to the direction of the spin polarization). Reversing the direction of the charge current changes the sign of recorded voltage. The reversal of the contact magnetization should lead to a hysteresis loop of the spin voltage of the ferromagnetic contact. The measured spin voltage amplitude is given by $\Delta V = \alpha \frac{\gamma P_{FM} E_F P_{SS}}{2e}$, where $\alpha = \sigma_{SS}/\sigma_{Total}$, σ_{SS} (σ_{Total}) is the surface (total) conductance, γ is the efficiency of spin detection of the contact, $P_{FM} = n_\uparrow - n_\downarrow / n_\uparrow + n_\downarrow$ is the spin polarization of the contact, $n_\uparrow$ ($n_\downarrow$) is the electron density for majority (minority) spin direction, and $P_{SS} = n_{SS\uparrow} - n_{SS\downarrow} / n_{SS\uparrow} + n_{SS\downarrow}$ is the spin polarization of the surface states [14,23]. ΔV is the voltage difference between the majority and minority spin carrier induced voltages measured at the detector terminals. The difference $\Delta V_{SPP} - \Delta V_{bare}$ before and after the SPPs excitation gives the measure of the net spin related signal.

VI. CONCLUSION

We show that carriers generated after decay of SPPs in an adiabatic conical Ag waveguide with the tip size of a few nanometers can be transferred to the surface of 3D TI such as Bi_2Se_3. We calculate the spin polarization current density due to hot carriers on the surface of 3D TI and provide a scheme for an experimental measurement of such currents. Our calculated value of the spin polarized current is of the order of 10^4 A/cm^2, and this result agrees with the experimentally measured value of spin polarized current on the surface of 3D TI. Our results can be useful for optical generation of enhanced spin polarizations and corresponding currents that can be useful in spintronics.

ACKNOWLEDGMENTS

Support for H.P.P. was provided by Grant No. DESC0007043 from the Physical Behavior of Materials Program, Office of Basic Energy Sciences, U.S. Department of Energy. V.A.'s work was supported by NSF Grant No. ECCS-1308473. For M.I.S.'s work, the support was provided by MURI Grant No. N00014-13-1-0649 from the U.S. Office of Naval Research.

[1] I. Goykhman, B. Desiatov, J. Khurgin, J. Shappir, and U. Levy, Nano Lett. **11**, 2219 (2011).
[2] M. W. Knight, H. Sobhani, P. Nordlander, and N. J. Halas, Science **332**, 702 (2011).
[3] A. Giugni B. Torre, A. Toma1, M. Francardi, M. Malerba, A. Alabastri, R. Proietti Zaccaria, M. I. Stockman and E. Di Fabrizio, Nat. Nanotechnol. **8**, 845 (2013).
[4] S. Mukherjee, F. Libisch, N. Large, O. Neumann, L. V. Brown, J. Cheng, J. B. Lassiter, E. A. Carter, P. Nordlander, and N. J. Halas, Nano Lett. **13**, 240 (2012).
[5] A. O. Govorov, H. Zhang, and Y. K. Gun'ko, J. Phys. Chem. C **117**, 16616 (2013).
[6] A. J. Babadjanyan, N. L. Margaryan, and K. V. Nerkararyan, J. Appl. Phys. **87**, 3785 (2000).
[7] M. I. Stockman, Phys. Rev. Lett. **93**, 137404 (2004).
[8] M. I. Stockman, Phys. Rev. Lett. **106**, 019901(E) (2011).
[9] H. P. Paudel, V. Apalkov, and M. I. Stockman, Phys. Rev. B **93**, 155105 (2016).
[10] A. C. Jones, R. L. Olmon, S. E. Skrabalak, B. J. Wiley, Y. N. Xia, and M. B. Raschke, Nano Lett. **9**, 2553 (2009).
[11] J. Saxler, J. Gomez Rivas, C. Janke, H. P. M. Pellemans, P. H. Bolivar, and H. Kurz, Phys. Rev. B **69**, 155427 (2004).
[12] M. Bernardi, J. Mustafa, J. B. Neaton, and S. G. Louie, Nat. Commun. **6**, 7044 (2015).
[13] I. Appelbaum, H. D. Drew, and M. S. Fuhrer, Appl. Phys. Lett. **98**, 023103 (2011).
[14] J. Tang, L.-T. Chang, X. Kou, K. Murata, E. S. Choi, M. Lang, Y. Fan, Y. Jiang, M. Montazeri, W. Jiang, Y. Wang, L. He, and K. L. Wang, Nano Lett. **14**, 5423 (2014).
[15] H. P. Paudel and M. N. Leuenberger, J. Phys.: Condens. Matter **26**, 082201 (2014).
[16] H. P. Paudel and M. N. Leuenberger, *Faraday Effect Due to Pauli Exclusion Principle in 3D Topological Insulator Nanostructures, Quantum Information and Computation XII* (Proc. SPIE, Baltimore, MA, 2014), p. 91230E.
[17] H. P. Paudel, Ph.D. thesis, University of Central Florida, Electronic Theses and Dissertations, 2014, http://stars.library.ucf.edu/etd/4737.
[18] M. Z. Hasan and C. L. Kane, Rev. Mod. Phys. **82**, 3045 (2010).
[19] D. Hsieh, Y. Xia, D. Qian, L. Wray, J. H. Dil, F. Meier, J. Osterwalder, L. Patthey, J. G. Checkelsky, N. P. Ong, A. V. Fedorov, H. Lin, A. Bansil, D. Grauer, Y. S. Hor, R. J. Cava, and M. Z. Hasan, Nature (London) **460**, 1101 (2009).
[20] R. Sundararaman, P. Narang, A. S. Jermyn, W. A. Goddard III, and H. A. Atwater, Nat. Commun. **5**, 5788 (2014).
[21] G. D. J. Smit, G. D. J, S. Rogge, and T. M. Klapwijk, Appl. Phys. Lett. **81**, 3852 (2002).
[22] Y. Q. Xia, Ph.D. thesis, Dissertation Abstracts International, 71-07, p 116 (2010); D. Hsieh (private communication) (2016).
[23] C. H. Li, O. M. J. van't Erve, S. Rajput, L. Li, and B. T. Jonker, Nat. Nanotech. **9**, 218 (2014).
[24] C. D. Spataru and F. Leonard, Phys. Rev. B **90**, 085115 (2014).
[25] Y. H. Wang, D. Hsieh, E. J. Sie, H. Steinberg, D. R. Gardner, Y. S. Lee, P. Jarillo-Herrero, and N. Gedik, Phys. Rev. Lett. **109**, 127401 (2012).
[26] J. A. Sobota, S. Yang, J. G. Analytis, Y. L. Chen, I. R. Fisher, P. S. Kirchmann, and Z.-X. Shen, Phys. Rev. Lett. **108**, 117403 (2012).
[27] J. A. Sobota, S.-L. Yang, A. F. Kemper, J. J. Lee, F. T. Schmitt, W. Li, R. G. Moore, J. G. Analytis, I. R. Fisher, P. S. Kirchmann, T. P. Devereaux, and Z.-X. Shen, Phys. Rev. Lett. **111**, 136802 (2013).
[28] K. Blum, *Density Matrix Theory and Applications* (Springer, Berlin, Heidelberg, 2012).

[29] J. Bosbach, C. Hendrich, F. Stietz, T. Vartanyan, and F. Trager, Phys. Rev. Lett. **89**, 257404 (2002).

[30] M. Durach, A. Rusina, and M. I. Stockman, Phys. Rev. Lett. **103**, 186801 (2009).

[31] N. W. Ashcroft and N. D. Mermin, *Solid State Physics* (Saunders College Publishing, Philadelphia, 1976), p. 68.

[32] R. H. Silsbee, J. Phys.: Condens. Matter **16**, R179 (2004).

[33] X. Lou, C. Adelmann, S. A. Crooker, E. S. Garlid, J. Zhang, K. S. Madhukar Reddy, S. D. Flexner, C. J. Palmstrom, and P. A. Crowell, Nat. Phys. **3**, 197 (2007).

[34] M. Johnson and R. H. Silsbee, Phys. Rev. Lett. **55**, 1790 (1985).